

Full-Sky Search for Ultra High Energy Cosmic Ray Anisotropies

Luis Anchordoqui¹, Carlos Hojvat², Thomas McCauley¹,
Thomas Paul¹, Stephen Reucroft¹, John Swain¹, and Allan Widom¹

¹ *Department of Physics, Northeastern University, Boston, MA 02115*

² *Fermi National Accelerator Laboratory, P.O. Box 500, Batavia, IL 60510*

Using data from the SUGAR and the AGASA experiments taken during a 10 yr period with nearly uniform exposure to the entire sky, we search for large-scale anisotropy patterns in the arrival directions of cosmic rays with energies $> 10^{19.6}$ eV. We determine the angular power spectrum from an expansion in spherical harmonics for modes out to $\ell = 5$. Based on available statistics, we find no significant deviation from isotropy. We compare the rather modest results which can be extracted from existing data samples with the results that should be forthcoming as new full-sky observatories begin operation.

I. INTRODUCTION

Ultra high energy cosmic rays are one of the most enigmatic phenomena in the universe. Despite the fact that the existence of particles with energies $\gtrsim 10^{20}$ eV has been known for over 40 years, their origin continues to be an intriguing puzzle [1]. The distribution of arrival directions is perhaps the most helpful observable in yielding clues about cosmic ray origin. On the one hand, if cosmic rays cluster within a small angular region [2] or show directional alignment with powerful compact objects [3], one might be able to associate them with isolated sources in the sky. On the other hand, if the distribution of arrival directions exhibits a large-scale anisotropy, this could indicate whether or not certain classes of sources are associated with large-scale structures (such as the Galactic plane or the Galactic halo). In this paper, we focus our attention on the search for such large-scale celestial patterns.

Cosmic ray air shower detectors which experience stable operation over a period of a year or more will have a uniform exposure in right ascension, α . A traditional technique to search for large-scale anisotropies is then to fit the right ascension distribution of events to a sine wave with period $2\pi/m$ (m^{th} harmonic) to determine the components (x, y) of the Rayleigh vector [4]

$$x = \frac{2}{N} \sum_{i=1}^N \cos(m\alpha_i), \quad y = \frac{2}{N} \sum_{i=1}^N \sin(m\alpha_i). \quad (1)$$

The m^{th} harmonic amplitude of N measurements α_i is given by the Rayleigh vector length $\mathcal{R} = (x^2 + y^2)^{1/2}$. The expected length of such vector for values randomly sampled from a uniform phase distribution is $\mathcal{R}_0 = 2/\sqrt{N}$. The chance probability of obtaining an amplitude with length larger than that measured is $p(\geq \mathcal{R}) = e^{-k_0}$, where $k_0 = \mathcal{R}^2/\mathcal{R}_0^2$. To give a specific example, a vector of length $k_0 \geq 6.6$ would be required to claim an observation whose probability of arising from random fluctuation was 0.0013 (a “ 3σ ” result). For the ultra high energy ($\gtrsim 10^{19.6}$ eV) regime, all experiments to date have reported $k_0 \ll 6.6$ [5]. This does not imply

an isotropic distribution, but it merely means that available data are too sparse to claim a statistically significant measurement of anisotropy by any of these experiments. In other words, there may exist anisotropies at a level too low to discern given existing statistics [6].

The right harmonic analyses are completely blind to intensity variations which depend only on declination, δ . Combining anisotropy searches in α over a range of declinations could dilute the results, since significant but out of phase Rayleigh vectors from different declination bands can cancel each other out. Moreover, the analysis methods that consider distributions in one celestial coordinate, while integrating away the second, have proved to be potentially misleading [7]. An unambiguous interpretation of anisotropy data requires two ingredients: *exposure to the full celestial sphere and analysis in terms of both celestial coordinates*. Though the statistics are very limited at present, this article describes a first step in this direction. In the next section we combine data from the Sydney University Giant Air-shower Recorder (SUGAR) and the Akeno Giant Air Shower Array (AGASA) taken during a 10 yr period with nearly uniform exposure to the entire sky. After that, in Sec. III, we apply the power spectrum estimation technique [8] to interpret the distribution of arrival directions. Our conclusions are collected in Sec. IV.

II. EXPERIMENTAL DATA SETS

The SUGAR array was operated from January 1968 to February 1979 in New South Wales (Australia) at a latitude of 30.5° South and longitude $149^\circ 38'$ East [9]. The array consisted of 47 independent stations on a rectangular grid covering an area $S \approx 70$ km². The primary energy was determined from the total number of muons, N_μ , traversing the detector at the measured zenith angle θ . The total aperture for incident zenith angles between θ_1 and θ_2 was found to be

$$A = \int_{\theta_1}^{\theta_2} S p(N_\mu, \theta) \cos \theta d\Omega. \quad (2)$$

Here, $p(N_\mu, \theta)$ is the probability that a shower falling within the physical area was detected, $S \cos \theta$ is the projected surface of the array in the shower plane, and $d\Omega$ is the acceptance solid angle. The SUGAR Collaboration reports [9] a reasonable accuracy in assessing the shower parameters up to $\theta = 73^\circ$. The particulars of the events with primary energy $> 10^{19.6}$ eV are given in Table I. The estimated angular uncertainty for showers that triggered 5 or more stations is reported as $3^\circ \sec \theta$ [9]. However, the majority of events were only viewed by 3 or 4 stations, and for these the resolution appears to be as poor as 10° [10]. Of particular interest for this analysis, $p(N_\mu > 10^8, \theta < 55^\circ) \approx 0.85$ [11], yielding a total aperture $A \approx 125 \text{ km}^2 \text{ sr}$. This provides an exposure reasonably matched to that of AGASA, which is described next.

The AGASA experiment occupies farm land near the village of Akeno (Japan) at a longitude of $138^\circ 30'$ East and latitude $35^\circ 30'$ North [12]. The array, which consists of 111 surface detectors deployed over an area of about 100 km^2 , has been running since 1990. About 95% of the surface detectors were operational from March to December 1991, and the array has been fully operational since then. A prototype detector operated from 1984 to 1990 and has been part of AGASA since 1990 [13]. The aperture for events with primary zenith angle $0^\circ < \theta < 45^\circ$ and energies beyond $10^{19.25}$ eV is found to be $A \approx 125 \text{ km}^2 \text{ sr}$ [12]. The angular resolution for these events is 1.6° [14]. The arrival directions of cosmic rays with energy $> 10^{19.6}$ eV are given in Table II.

The expected event rate is found to be

$$\begin{aligned} \frac{dN}{dt} &= A \int_{E_1}^{E_2} E^3 J(E) \frac{dE}{E^3} \\ &\approx \frac{A}{2} \langle E^3 J(E) \rangle \left[\frac{1}{E_1^2} - \frac{1}{E_2^2} \right], \end{aligned} \quad (3)$$

where $\langle E^3 J(E) \rangle \approx 10^{24.6} \text{ eV}^2 \text{ m}^{-2} \text{ s}^{-1} \text{ sr}^{-1}$ stands for the observed ultra high energy cosmic ray flux, which has a cutoff at $E_2 = 10^{20.5}$ eV [1]. Thus, in approximately 10 yr of running each of these experiments should collect ≈ 50 events above $E_1 = 10^{19.6}$ eV, arriving with a zenith angle $< \theta_{\max}$. Here, $\theta_{\max} = 45^\circ$ for AGASA and $\theta_{\max} = 55^\circ$ for SUGAR. Our sub-sample for the full-sky anisotropy search consists of the 50 events detected by AGASA from May 1990 to May 2000 [6], and the 49 events detected by SUGAR with $\theta < 55^\circ$ [11]. Note that we consider the full data sample for the 11 yr lifetime of SUGAR (in contrast to the 10 yr data sample from AGASA). This roughly compensates for the time variation of the sensitive area of the experiment as detectors were deployed or inactivated for maintenance. The arrival directions of the 99 events are plotted in Fig. 1 (equatorial coordinates B.1950).

A detector at latitude a_0 that has continuous operation with constant exposure in right ascension and is fully efficient for $\theta < \theta_{\max}$ has relative exposure with the following dependence on declination [15]

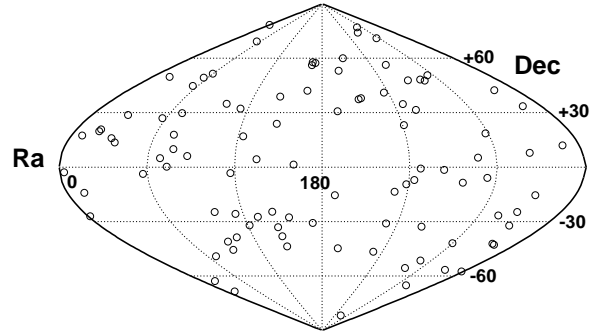


FIG. 1. Arrival direction of the 99 events observed above $10^{19.6}$ eV by the SUGAR ($\theta < 55^\circ$) and the AGASA ($\theta < 45^\circ$) experiments (equatorial coordinates B.1950).

$$\omega(\delta) \propto (\cos a_0 \cos \delta \sin \alpha_{\max} + \alpha_{\max} \sin a_0 \sin \delta), \quad (4)$$

where α_{\max} , the local hour angle at which the zenith angle becomes equal to θ_{\max} , is given by

$$\alpha_{\max} = \begin{cases} 0 & \text{if } \xi > 1 \\ \pi & \text{if } \xi < -1 \\ \cos^{-1} \xi & \text{otherwise} \end{cases} \quad (5)$$

with

$$\xi \equiv \frac{\cos \theta_{\max} - \sin a_0 \sin \delta}{\cos a_0 \cos \delta}. \quad (6)$$

We normalize the relative exposure by scaling the declination angle dependence given in Eq. (4) by an estimate of the areas and operation times for SUGAR and AGASA (recall that the stated area of SUGAR is an overestimate, and this compensated to some degree by the longer running time). The result, displayed in Fig. 2, shows that the combined exposure of these arrays is nearly uniform over the entire sky.

III. CORRELATIONS AND POWER SPECTRUM

We begin this section with a general introduction to the calculation of the angular power spectrum and the determination of the expected size of intensity fluctuations. The technique is then applied to the AGASA and SUGAR data in order to check for fluctuations beyond those expected from an isotropic distribution.

Let us start by defining the directional phase space of the angular distribution of cosmic ray events in equatorial coordinates, (α, δ) . (i) The direction of the event is described by a unit vector

$$\mathbf{n} = \sin \delta (\mathbf{i} \cos \alpha + \mathbf{j} \sin \alpha) + \mathbf{k} \cos \delta; \quad (7)$$

(ii) The solid angle is given by

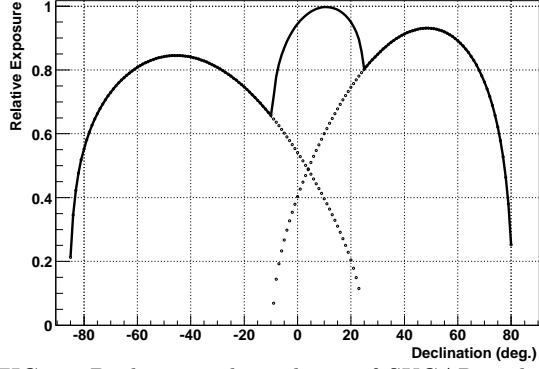


FIG. 2. Declination dependence of SUGAR and AGASA relative exposures (dotted). The solid line indicates the combined declination dependence of the relative exposure.

$$d^2 \mathbf{n} = \sin \delta \, d\delta \, d\alpha ; \quad (8)$$

(iii) The delta function for the solid angle is defined as

$$\delta(\mathbf{n}, \mathbf{n}') = \delta(\cos \delta - \cos \delta') \sum_{m=-\infty}^{\infty} \delta(\alpha - \alpha' + 2\pi m), \quad (9)$$

so that, as usual,

$$f(\mathbf{n}) = \int \delta(\mathbf{n}, \mathbf{n}') f(\mathbf{n}') d^2 \mathbf{n}' ; \quad (10)$$

(iv) The probability distribution $P(\mathbf{n})d^2 \mathbf{n}$ of events can be employed for the purpose of computing the averages

$$\bar{f} = \int f(\mathbf{n}) P(\mathbf{n}) d^2 \mathbf{n} ; \quad (11)$$

Finally, (v) for a sequence of N different cosmic ray events $(\mathbf{n}_1, \dots, \mathbf{n}_N)$ one may assume an independent distributions for each event, i.e.

$$P_N(\mathbf{n}_1, \dots, \mathbf{n}_N) \prod_i d^2 \mathbf{n}_i = \prod_i \{P(\mathbf{n}_i) d^2 \mathbf{n}_i\} . \quad (12)$$

For a sequence of events $(\mathbf{n}_1, \dots, \mathbf{n}_N)$ let us describe the angular intensity as the random variable

$$I(\mathbf{n}) = \frac{1}{N} \sum_{j=1}^N \delta(\mathbf{n}, \mathbf{n}_j) . \quad (13)$$

From Eqs. (12) and (13) it follows that

$$\begin{aligned} \overline{I(\mathbf{n})} &= \int \dots \int I(\mathbf{n}) P_N(\mathbf{n}_1, \dots, \mathbf{n}_N) \prod_i d^2 \mathbf{n}_i \\ &= P(\mathbf{n}). \end{aligned} \quad (14)$$

The two point correlation function $G(\mathbf{n}, \mathbf{n}') = \overline{I(\mathbf{n})I(\mathbf{n}')}$ is defined via

$$\begin{aligned} G(\mathbf{n}, \mathbf{n}') &= \int \dots \int I(\mathbf{n}) I(\mathbf{n}') P_N(\mathbf{n}_1, \dots, \mathbf{n}_N) \prod_i d^2 \mathbf{n}_i \\ &= \frac{1}{N} \delta(\mathbf{n}, \mathbf{n}') P(\mathbf{n}) + \left(1 - \frac{1}{N}\right) P(\mathbf{n}) P(\mathbf{n}') . \end{aligned} \quad (15)$$

The “power spectrum” of the correlation function is determined by the eigenvalue equation

$$\int G(\mathbf{n}, \mathbf{n}') \psi_\lambda(\mathbf{n}') d^2 \mathbf{n}' = \lambda \psi_\lambda(\mathbf{n}). \quad (16)$$

In this regard it is useful to introduce Dirac notation to indicate the inner product

$$\langle \psi | \psi \rangle = \int \psi^*(\mathbf{n}) \psi(\mathbf{n}) d^2 \mathbf{n} . \quad (17)$$

With this in mind, Eq. (16) reads

$$G |\psi_\lambda\rangle = \lambda |\psi_\lambda\rangle . \quad (18)$$

In the limit of a large number of events $N \rightarrow \infty$,

$$\lim_{N \rightarrow \infty} G(\mathbf{n}, \mathbf{n}') \equiv G_\infty(\mathbf{n}, \mathbf{n}') = P(\mathbf{n})P(\mathbf{n}'), \quad (19)$$

or equivalently,

$$\hat{G}_\infty = |P\rangle \langle P| . \quad (20)$$

In such a limit, fluctuations can be neglected and we find only *two possible values* in the spectrum: (i) There is a non-degenerate non-zero eigenvalue

$$\hat{G}_\infty |P\rangle = \lambda_\infty |P\rangle , \quad (21)$$

with

$$\lambda_\infty = \langle P|P\rangle = \int P^2(\mathbf{n}) d^2 \mathbf{n}. \quad (22)$$

(ii) For every state $|f\rangle$ orthogonal to $|P\rangle$ with mean value $\bar{f} = \langle P|f\rangle = 0$, there exists a *zero eigenvalue* in the power spectrum

$$\hat{G}_\infty |f\rangle = |P\rangle \langle P|f\rangle = \left\{ \int P f d^2 \mathbf{n} \right\} |P\rangle = \bar{f} |P\rangle = 0 . \quad (23)$$

Let us now turn to consider the effects of finite N . Defining the fluctuations in the intensity by

$$\Delta I(\mathbf{n}) = I(\mathbf{n}) - \overline{I(\mathbf{n})} = I(\mathbf{n}) - P(\mathbf{n}), \quad (24)$$

the two point correlation function can be re-written as

$$\begin{aligned} G(\mathbf{n}, \mathbf{n}') &= \overline{I(\mathbf{n})I(\mathbf{n}')} = \overline{I(\mathbf{n})} \overline{I(\mathbf{n}')} + \overline{\Delta I(\mathbf{n})\Delta I(\mathbf{n}')} \\ &= G_\infty(\mathbf{n}, \mathbf{n}') + \overline{\Delta I(\mathbf{n})\Delta I(\mathbf{n}')}, \end{aligned} \quad (25)$$

with

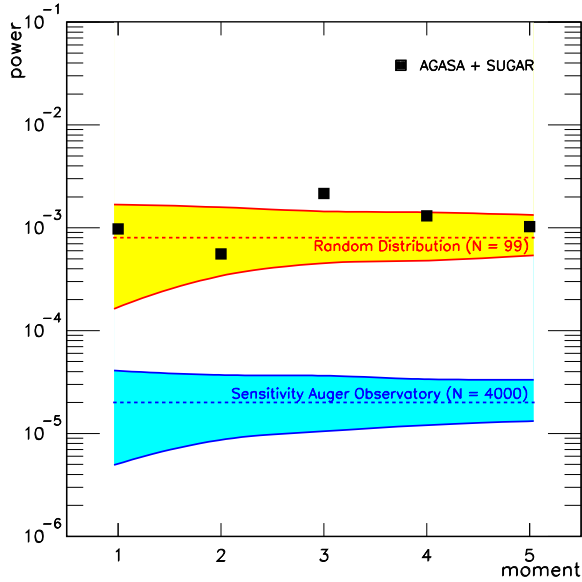


FIG. 3. The angular power spectrum is indicated by the squares. The horizontal lines indicate the mean value, $\overline{C}(\ell) = (4\pi N)^{-1}$, expected for an isotropic distribution. The upper shaded band shows the 1σ fluctuation around the mean value for $N = 99$. The band was obtained from 1000 sets of Monte Carlo simulations of 99 events each, including small corrections for ω_j . The results from the Monte Carlo are consistent with the errors computed using Eq. (48) for the case of $\omega_j = 1$. For $\ell = 3$, where there is a small excess compared to the expectation for isotropy, $C(3) = 2.16 \times 10^{-3}$ while the expectation from a random distribution is $\overline{C}_{MC}(3) = 9.5 \times 10^{-4}$, with a variance of 5.0×10^{-4} . The projected sensitivity for the Pierre Auger Observatory is also indicated on the plot by the lower shaded band.

$$\overline{\Delta I(\mathbf{n})\Delta I(\mathbf{n}')} = \frac{1}{N} [\delta(\mathbf{n}, \mathbf{n}')P(\mathbf{n}) - P(\mathbf{n})P(\mathbf{n}')] , \quad (26)$$

where Eq. (15) has been invoked. Putting all this together, some general results follow: (i) For the $N \rightarrow \infty$ case, there is only one state with a finite eigenvalue λ_∞ , while the rest of the power spectrum corresponds to $\lambda = 0$. (ii) For finite N , Eq. (26) implies that the fluctuations are of order N^{-1} . The power spectrum for large N then has one eigenvalue of order unity and the rest of the eigenvalues are of order N^{-1} .

Now, for an isotropic distribution of \mathbf{n} ,

$$\tilde{P}(\mathbf{n}) = \frac{1}{4\pi} , \quad (27)$$

and the two point correlation function of Eq. (15) becomes,

$$\tilde{G}(\mathbf{n}, \mathbf{n}') = \frac{1}{4\pi N} \delta(\mathbf{n}, \mathbf{n}') + \frac{1}{(4\pi)^2} \left(1 - \frac{1}{N}\right) . \quad (28)$$

The eigenvalue problem is solved by employing spherical harmonics [17]

$$\int \tilde{G}(\mathbf{n}, \mathbf{n}') Y_{\ell m}(\mathbf{n}') d^2\mathbf{n}' = \lambda_{\ell m} Y_{\ell m}(\mathbf{n}) , \quad (29)$$

where from Eq. (28) we have,

$$\lambda_{\ell m} = \begin{cases} (4\pi)^{-1} & \text{if } (\ell, m) = (0, 0) \\ (4\pi N)^{-1} & \text{if } (\ell, m) \neq (0, 0) \end{cases} . \quad (30)$$

The eigenfunctions form a useful set for expansions of the intensity over the celestial sphere

$$I(\mathbf{n}) = \sum_{\ell=0}^{\infty} \sum_{m=-\ell}^{\ell} a_{\ell m} Y_{\ell m}(\mathbf{n}) . \quad (31)$$

To incorporate the dependence on declination given in Eq. (4), let us re-define the angular intensity

$$I(\mathbf{n}) = \frac{1}{\mathcal{N}} \sum_{j=1}^N \frac{1}{\omega_j} \delta(\mathbf{n}, \mathbf{n}_j) , \quad (32)$$

where ω_j is the relative exposure at arrival direction \mathbf{n}_j given in Fig. 2 and \mathcal{N} is the sum of the weights ω_j^{-1} . Since the eigenvalues of the $Y_{\ell m}$ expansion are uniquely defined

$$a_{\ell m} = \int I(\mathbf{n}) Y_{\ell m}(\mathbf{n}) d^2\mathbf{n} , \quad (33)$$

the replacement of Eq. (32) into Eq. (33) leads to the explicit form of the coefficients for our set of arrival directions

$$a_{\ell m} = \frac{1}{\mathcal{N}} \sum_{j=1}^N \frac{1}{\omega_j} Y_{\ell m}(\mathbf{n}_j) . \quad (34)$$

Squaring Eq. (34) and taking the average yields

$$\overline{a_{\ell m}^2} = \frac{\delta_{\ell 0} \delta_{m 0}}{4\pi} + \frac{1}{4\pi N} (1 - \delta_{\ell 0} \delta_{m 0}) . \quad (35)$$

Equivalently, the mean square fluctuations of the coefficients are determined by the power spectrum eigenvalues according to

$$\overline{a_{\ell m}^2} = \lambda_{\ell m} . \quad (36)$$

Although full anisotropy information is encoded into the coefficients $a_{\ell m}$ (tied to some specified coordinate system), the (coordinate independent) total power spectrum of fluctuations

$$C(\ell) = \frac{1}{(2\ell+1)} \sum_{m=-\ell}^{\ell} a_{\ell m}^2 , \quad (37)$$

provides a gross summary of the features present in the celestial distribution together with the characteristic angular scale(s). Note that Eqs. (30) and (36) imply

$$\overline{C}(\ell) = \frac{1}{(2\ell+1)} \sum_{m=-\ell}^{\ell} \overline{a_{\ell m}^2} = \begin{cases} (4\pi)^{-1} & \text{if } \ell = 0 \\ (4\pi N)^{-1} & \text{if } \ell \neq 0 \end{cases}. \quad (38)$$

One must take care when combining data from experiments with differing angular resolutions, as in the case for SUGAR and AGASA. In this analysis, we consider only anisotropy on an angular scale larger than the resolution of SUGAR, which has the worse resolution of the two. The power in mode ℓ is sensitive to variation over angular scales of ℓ^{-1} radians [15]. Recalling that the estimated angular uncertainty for some of the events in the SUGAR sample is possibly as poor as 10° [10] we only look in this study for large scale patterns, going into the multipole expansion out to $\ell = 5$.

Our results at this juncture are summarized in Fig. 3. The angular power spectrum is consistent with that expected from a random distribution for all (analyzed) multipoles, though there is a small (2σ) excess in the data for $\ell = 3$. The majority of this excess comes from SUGAR data [18]. The decrease in error as ℓ increases may be understood as a consequence of the fact that contributions to mode ℓ arise from variations over an angular scale ℓ^{-1} . If one compares to the expectation for isotropy, structures characterized by a smaller angular scale, and hence larger ℓ , can be ruled out with more significance than larger structures.

To quantify the error, we study the fluctuations in $C(\ell)$ for $\ell \geq 1$. For simplicity, let us neglect the small effects of declination (*viz.*, $\omega_j = 1 \forall j$), and consider the random variable

$$X_\ell = \frac{C(\ell)}{\overline{C}(\ell)} = \left(\frac{4\pi N}{2\ell+1} \right) \sum_{m=-\ell}^{\ell} a_{\ell m}^2. \quad (39)$$

Denoting by $P_\ell(\cos \delta)$ the Legendre polynomial of order ℓ and employing the addition theorem for spherical harmonics,

$$\frac{4\pi}{2\ell+1} \sum_{m=-\ell}^{\ell} Y_{\ell m}(\mathbf{n}) Y_{\ell m}(\mathbf{n}') = P_\ell(\mathbf{n} \cdot \mathbf{n}'), \quad (40)$$

Eqs. (34), (39), and (40) imply that

$$X_\ell = 1 + \frac{2}{N} \sum_{1 \leq i < j \leq N} P_\ell(\mathbf{n}_i \cdot \mathbf{n}_j), \quad (41)$$

where $P_\ell(1) = 1$ has been invoked. Evidently, $\overline{X}_\ell = 1$. Besides,

$$\overline{X_\ell^2} = 1 + \frac{4}{N^2} \sum_{1 \leq i < j \leq N} \sum_{1 \leq k < q \leq N} \overline{P_\ell(\mathbf{n}_i \cdot \mathbf{n}_j) P_\ell(\mathbf{n}_k \cdot \mathbf{n}_q)}. \quad (42)$$

Since different pairs in the sum on the right hand side of Eq. (42) are uncorrelated for an isotropic distribution, it follows that

$$\overline{X_\ell^2} = 1 + \frac{4}{N^2} \sum_{1 \leq i < j \leq N} \overline{P_\ell(\mathbf{n}_i \cdot \mathbf{n}_j)^2}. \quad (43)$$

There are $\{N(N-1)/2\}$ equivalent pairs in Eq. (43) which implies

$$\overline{X_\ell^2} = \overline{X_\ell^2} + 2 \left(1 - \frac{1}{N} \right) \overline{P_\ell(\mathbf{n}_1 \cdot \mathbf{n}_2)^2}. \quad (44)$$

From Eq. (40) we obtain

$$\begin{aligned} \overline{P_\ell(\mathbf{n}_1 \cdot \mathbf{n}_2)^2} &= \left(\frac{4\pi}{2\ell+1} \right)^2 \sum_{m=-\ell}^{\ell} \overline{Y_{\ell m}(\mathbf{n}_1)^2} \overline{Y_{\ell m}(\mathbf{n}_2)^2} \\ &= \frac{1}{2\ell+1}. \end{aligned} \quad (45)$$

Plugging Eq. (45) into Eq. (44) leads to

$$\overline{\Delta X_\ell^2} = \left(1 - \frac{1}{N} \right) \frac{2}{2\ell+1}, \quad (46)$$

or equivalently,

$$\left(\frac{\overline{\Delta C_\ell^2}}{\overline{C_\ell^2}} \right) = \left(1 - \frac{1}{N} \right) \frac{2}{2\ell+1}, \quad (47)$$

yielding (for large N)

$$\lim_{N \rightarrow \infty} \left(\frac{\overline{\Delta C_\ell^2}}{\overline{C_\ell^2}} \right) = \frac{2}{2\ell+1} \quad \text{for } \ell \geq 1, \quad (48)$$

which is the variance on X_ℓ .

IV. OUTLOOK

We have made a first full-sky anisotropy search using data from the SUGAR and AGASA experiments. At present, low statistics and poor angular resolution limits our ability to perform a very sensitive survey, but we can at least have a preliminary look at the first moments in the angular power spectrum. The data are consistent with isotropy, though there appears to be a small excess for $\ell = 3$, arising mostly from the SUGAR data.

There are two caveats in this analysis which should be kept in mind. First, from the published SUGAR results, it is difficult to make an exact determination of the exposure, as the sensitive area of the experiment varied as a function of time. Here, we assumed an area-time product of approximately $775 \text{ km}^2 \text{ yr}$. Second, there is some uncertainty in the energy calibration. The SUGAR results are reported in terms of the number of vertical equivalent muons together with two possible models to convert this to primary energy. We have chosen the model yielding an energy spectrum which is in better agreement with the AGASA results [19]. It should be noted, though, that this spectrum does not agree well with the results of the High

Resolution Fly's Eye (HiRes) experiment [20]. Though there are uncertainties in the energy scale, the impact on this anisotropy search may not be so severe. This is because the energy cut of $10^{19.6}$ eV is well above the last break in the spectral index at $\sim 10^{18.5} - 10^{19}$ eV, and one would expect that all cosmic rays above this break share similar origins.

In the near future we expect dramatically superior results from the Pierre Auger Observatory. This observatory is designed to measure the energy and arrival direction of ultra high energy cosmic rays with unprecedented precision. It will consist of two sites, one in the Northern hemisphere and one in the Southern, each covering an area $S \approx 3000$ km². The Southern site is currently under construction while the Northern site is pending. Once complete, these two sites together will provide the full sky coverage and well matched exposures which are crucial for anisotropy analyses. The base-line design of the detector includes a ground array consisting of 1600 water Čerenkov detectors overlooked by 4 fluorescence eyes. The angular and energy resolutions of the ground arrays are typically less than 1.5° (multi-pole expansion $\ell \sim 60$) and less than 20%, respectively. The detectors are designed to be fully efficient ($p \approx 1$) out to $\theta_{\max} = 60^\circ$ beyond 10^{19} eV, yielding a nearly uniform sky $A \approx 1.4 \times 10^4$ km² sr [15]. In 10 yr of running the two arrays will collect ≈ 4000 events above $E_1 = 10^{19.6}$ eV. As can be seen from Fig. 3, such statistics will allow one to discern asymmetries at the level of about 1 in 10^4 .

ACKNOWLEDGMENTS

This work has been partially supported by the US National Science Foundation (NSF), under grant No. PHY-0140407.

-
- [1] For recent reviews see *e.g.*, P. Bhattacharjee and G. Sigl, Phys. Rept. **327**, 109 (2000) [arXiv:astro-ph/9811011]; M. Nagano and A. A. Watson, Rev. Mod. Phys. **72** (2000) 689; L. Anchordoqui, T. Paul, S. Reucroft and J. Swain, Int. J. Mod. Phys. A **18**, 2229 (2003) [arXiv:hep-ph/0206072].
 - [2] It is noteworthy that the world data set suggest that the pairing of events on the celestial sphere is occurring at a higher than chance coincidence. Y. Uchihori, M. Nagano, M. Takeda, M. Teshima, J. Lloyd-Evans and A. A. Watson, Astropart. Phys. **13** (2000) 151 [arXiv:astro-ph/9908193]. However, to calculate a meaningful statistical significance of this clustering, one must define the search procedure *a priori* in order to ensure it is not (inadvertently) devised especially to suite the particular data set after having studied it. In the above mentioned analysis the angular bin size was not defined ahead of time.
 - [3] See *e.g.*, G. R. Farrar and P. L. Biermann, Phys. Rev. Lett. **81**, 3579 (1998) [arXiv:astro-ph/9806242]; G. Sigl, D. F. Torres, L. A. Anchordoqui and G. E. Romero, Phys. Rev. D **63**, 081302 (2001) [arXiv:astro-ph/0008363]; A. Virmani, S. Bhattacharya, P. Jain, S. Razzaque, J. P. Ralston and D. W. McKay, Astropart. Phys. **17**, 489 (2002) [arXiv:astro-ph/0010235]; D. F. Torres, S. Reucroft, O. Reimer and L. A. Anchordoqui, Astrophys. J. Lett. (to be published) [arXiv:astro-ph/0307079].
 - [4] J. Linsley, Phys. Rev. Lett. **34**, 1530 (1975).
 - [5] D. M. Edge, A. M. Pollock, R. J. Reid, A. A. Watson and J. G. Wilson, J. Phys. G **4** (1978) 133; M. M. Winn, J. Ulrichs, L. S. Peak, C. B. Mccusker and L. Horton, J. Phys. G **12** (1986) 675; G. L. Cassiday *et al.*, Astrophys. J. **351**, 454 (1990); M. Takeda *et al.*, Astrophys. J. **522**, 225 (1999) [arXiv:astro-ph/9902239]. For the Fly's Eye data-sample the Rayleigh vector was computed using weighted showers, because it has had a nonuniform exposure in sidereal time. A shower's weight depends on the hour of its sidereal arrival time, and the 24 different weights are such that every time bin has the same weighted number of showers.
 - [6] See *e.g.*, N. W. Evans, F. Ferrer and S. Sarkar, Astropart. Phys. **17**, 319 (2002).
 - [7] J. Wdowczyk and A. W. Wolfendale, J. Phys. G **10** (1984) 1453.
 - [8] P. J. E. Peebles, Astrophys. J. **185**, 413 (1973); M. G. Hauser and P. J. E. Peebles, Astrophys. J. **185**, 757 (1973); M. Tegmark, D. H. Hartmann, M. S. Briggs and C. A. Meegan, Astrophys. J. **468** (1996) 214 [arXiv:astro-ph/9510129].
 - [9] M. M. Winn, J. Ulrichs, L. S. Peak, C. B. Mccusker and L. Horton, J. Phys. G **12** (1986) 653.
 - [10] R. W. Clay, R. Meyhandan, L. Horton, J. Ulrichs, and M. M. Winn, Astron. Astrophys. **255**, 167 (1992); L. J. Kewley, R. W. Clay and B. R. Dawson, Astropart. Phys. **5**, 69 (1996).
 - [11] C. J. Bell *et al.*, J. Phys. A **7** (1974) 990.
 - [12] N. Chiba *et al.*, Nucl. Instrum. Meth. A **311**, 338 (1992); H. Ohoka, S. Yoshida and M. Takeda [AGASA Collaboration], Nucl. Instrum. Meth. A **385**, 268 (1997).
 - [13] M. Teshima *et al.*, Nucl. Instrum. Meth. A **247**, 399 (1986).
 - [14] M. Takeda *et al.*, Phys. Rev. Lett. **81**, 1163 (1998) [arXiv:astro-ph/9807193].
 - [15] P. Sommers, Astropart. Phys. **14**, 271 (2001) [arXiv:astro-ph/0004016].
 - [16] N. Hayashida *et al.*, arXiv:astro-ph/0008102.
 - [17] Throughout this work we use real-valued spherical harmonics, which are obtained from the complex ones by substituting, $e^{im\phi} \rightarrow \sqrt{2}\sin(m\phi)$, if $m < 0$, $e^{im\phi} \rightarrow \sqrt{2}\cos(m\phi)$, if $m > 0$, and $e^{im\phi} \rightarrow 1$ if $m = 0$.
 - [18] C. Isola and G. Sigl, Phys. Rev. D **66**, 083002 (2002) [arXiv:astro-ph/0203273]; M. Kachelriess and D. V. Semikoz, arXiv:astro-ph/0306282.
 - [19] L. A. Anchordoqui, arXiv:hep-ph/0306078.
 - [20] T. Abu-Zayyad *et al.* [High Resolution Fly's Eye Collaboration], arXiv:astro-ph/0208243.

TABLE I. Arrival directions of cosmic rays with energy $> 10^{19.6}$ eV in equatorial coordinates (α, δ) together with the incident zenith angle (θ) as reported by the SUGAR Collaboration [9].

θ [deg.]	α [deg.]	δ [deg.]	θ [deg.]	α [deg.]	δ [deg.]	θ [deg.]	α [deg.]	δ [deg.]
70	187.5	31.8	27	333.0	-56.6	72	354.0	-75.2
28	117.0	-3.3	54	231.0	-31.0	43	357.0	-57.4
43	147.0	-43.6	34	130.5	-27.4	24	121.5	-32.0
31	105.0	-38.7	23	288.0	-51.4	64	204.0	24.0
29	231.0	-13.5	28	57.0	-3.7	35	261.0	-32.8
38	135.0	4.3	60	340.5	-43.2	51	300.0	-41.9
32	238.5	-9.5	38	16.5	-68.5	68	181.5	20.1
31	247.5	-0.7	33	331.5	-32.2	23	69	-49.1
40	280.5	-55.6	64	303	13.6	62	126.0	-39.9
55	226.5	-31.1	42	316.5	-65.1	45	189	-15.5
6	114	-25.8	14	145.5	-38.1	48	154.5	-27.7
53	268.5	-81.7	69	216	18.6	46	76.5	10
69	315	0.7	67	154.5	3.1	67	123	-38
23	277.5	-8.5	38	160.5	1.5	53	1.5	-27.1
54	337.5	-42.2	57	85.5	20.5	70	88.5	-64.6
64	303	-47.2	44	142.5	-24.6	52	172.5	-30.8
15	99	-24.7	49	30	15.9	49	73.5	0.2
58	355.5	-0.5	65	283.5	-50.6	42	19.5	-62.8
27	331.5	-15.5	15	144	-33.1	41	12	-14.1
68	163.5	-5.9	63	27	3.1	46	315	-26.6
56	234	1.2	43	94.5	-41	57	229.5	-78.7
72	117	-35.9	62	262.5	28.2	22	93	-45.6
59	223.5	-88.3	40	3	-2.9	33	195	-44.7
59	30	-78.5	38	327	-24.7	23	231	-46.6
52	340.5	-42.8	41	87	6.1	58	183	4.5
57	22.5	22.2	61	244.5	14.3	65	255	-83
57	88.5	-47.8	57	180	-22.7			

TABLE II. AGASA events with $\theta < 45^\circ$ and mean energy $> 10^{19.6}$ eV in equatorial coordinates (α, δ) based on the B.1950 reference frame. The first 2 rows refer to events measured using the prototype detector before 1990 [16].

α [deg.]	δ [deg.]	α [deg.]	δ [deg.]	α [deg.]	δ [deg.]	α [deg.]	δ [deg.]
334.70	38.15	276.80	35.26	68.71	30.00	210.03	50.14
328.68	27.36	206.45	34.95	86.65	58.48		
243.58	-7.08	236.31	41.15	284.40	47.73	53.01	69.33
287.03	77.12	2.29	78.32	143.23	38.82	267.68	47.91
7.85	17.42	255.27	31.47	171.55	57.37	100.17	34.95
123.54	16.95	208.34	60.04	28.28	28.75	18.25	49.74
18.07	20.83	280.91	48.25	73.27	17.92	167.77	57.87
263.60	-1.57	192.39	30.87	17.83	19.73	69.46	29.80
240.96	23.13	57.24	26.95	269.34	74.10	198.98	53.16
297.94	18.57	323.63	7.87	247.29	34.70	213.73	37.93
294.35	70.98	293.83	-5.91	33.82	13.57	166.55	42.07
146.04	23.93	258.77	56.35	167.52	56.27	348.37	12.03
293.67	50.59	55.38	44.74	287.13	5.22	113.95	32.31
55.59	49.34	345.16	33.63	339.45	42.34	68.59	5.00
59.55	51.56	211.47	37.34				